SIAM J. SCI. COMPUT.
Vol. 42, No. 3, pp. B738–B760

ADAPTIVE SECOND-ORDER CRANK–NICOLSON TIME-STEPPING SCHEMES FOR TIME-FRACTIONAL MOLECULAR BEAM EPITAXIAL GROWTH MODELS*

BINGQUAN JI†, HONG-LIN LIAO‡, YUEZHENG GONG†, AND LUMING ZHANG†

Abstract. Adaptive second-order Crank–Nicolson time-stepping methods using the recent scalar auxiliary variable (SAV) approach are developed for the time-fractional molecular beam epitaxial models with Caputo's fractional derivative. Based on the piecewise linear interpolation, the Caputo's derivative is approximated by a novel second-order formula, which is naturally suitable for a general class of nonuniform meshes and essentially preserves the positive semidefinite property of the integral kernel. The resulting Crank–Nicolson SAV time-stepping schemes are unconditionally energy stable on arbitrary nonuniform time meshes. The fast algorithm and adaptive time strategy are employed to speed up the numerical computation. Ample numerical results show that our methods are computationally efficient in multiscale time simulations and appropriate for accurately resolving the intrinsically initial singularity of the solution and for efficiently capturing the fast dynamics away from the initial time.

Key words. time-fractional molecular beam epitaxial, nonuniform L1-type formulas, scalar auxiliary variable approach, unconditional energy stability, adaptive time-stepping method

AMS subject classifications. 35Q99, 65M06, 65M12, 74A50

DOI. 10.1137/19M1259675

1. Introduction.

The molecular beam epitaxial (MBE) growth models, in recent years, have become a powerful new technique in material science, such as making compound semiconductor manufacture with great precision and high purity. Also, this technique is broadly applied to investigate thin-film deposition of single crystal. Roughly speaking, the mathematical models used in previous works to study dynamics of the MBE growth process can be classified into three broad categories: atomistic models that are performed using the form of molecular dynamics [4], continuum models in the form of partial differential systems [29], and hybrid models [8] which can be regarded as a compromise in the light of the models mentioned above.

We are interested in the continuum model for the evolution of the MBE growth that is derived by energy variational strategy. More precisely, the Ehrlich–Schwoebel energy is given as

$$E[\phi] = \int_\Omega \left(\frac{\varepsilon^2}{2} |\Delta\phi|^2 + F(\nabla\phi) \right) \mathrm{d}\mathbf{x}, \tag{1.1}$$

in which ϕ is a scaled height function of a thin film, $\varepsilon > 0$ is a positive constant, and $F(\mathbf{v})$ is a nonlinear, smooth function of its argument $\mathbf{v} \in \mathbb{R}^d\,(d = 1, 2, 3)$. There are

*Submitted to the journal's Computational Methods in Science and Engineering section May 6, 2019; accepted for publication (in revised form) April 13, 2020; published electronically June 1, 2020. https://doi.org/10.1137/19M1259675

Funding: The work of the second author was supported by the NUAA Scientific Research Starting Fund of Introduced Talent through grant 1008-56SYAH18037. The work of the third author was partially supported by the NSFC through grant 11801269, by the NSF through grant BK20180413, and by the Foundation of Jiangsu Key Laboratory for Numerical Simulation of Large Scale Complex Systems (202002). The work of fourth author was supported by the NSFC through grant 11571181.

†Department of Mathematics, Nanjing University of Aeronautics and Astronautics, 211101, P. R. China (jibingquanm@163.com, gongyuezheng@nuaa.edu.cn, zhanglm@nuaa.edu.cn).

‡Corresponding author. Department of Mathematics, Nanjing University of Aeronautics and Astronautics, Nanjing 211106, P. R. China (liaohl@csrc.ac.cn).

two popular choices of the nonlinear bulk potential: the double well potential, $F(\mathbf{v}) = \frac{1}{4}(|\mathbf{v}|^2 - 1)^2$, for the case of slope selection model, and the logarithmic potential, $F(\mathbf{v}) = -\frac{1}{2}\ln(1 + |\mathbf{v}|^2)$, for the case without slope selection model. The height evolution model can be derived as an L^2 gradient flow associated with the effective energy functional $E[\phi]$, i.e.,

$$\partial_t \phi = -M \frac{\delta E}{\delta \phi} = -M \left(\varepsilon^2 \Delta^2 \phi - \nabla \cdot f(\nabla \phi) \right), \tag{1.2}$$

in which the positive constant M is the mobility coefficient, and the case of slope selection model, $f(\mathbf{v}) = (|\mathbf{v}|^2 - 1)\mathbf{v}$, and the case without slope selection model, $f(\mathbf{v}) = -\mathbf{v}/(1 + |\mathbf{v}|^2)$. One intrinsic property of the above system is the energy dissipation law,

$$\frac{\mathrm{d}E}{\mathrm{d}t} = \left(\frac{\delta E}{\delta \phi}, \frac{\partial \phi}{\partial t} \right) = -\frac{1}{M} \|\partial_t \phi\|^2 \leqslant 0, \tag{1.3}$$

where the L^2 inner product is defined by $(f, g) = \int_\Omega fg \, \mathrm{d}\mathbf{x}$ and the associated L^2 norm $\|f\| = \sqrt{\int_\Omega f^2 \, \mathrm{d}\mathbf{x}}$ for all $f, g \in L^2(\Omega)$. Notice that the periodic boundary condition or any other proper boundary that can satisfy the flux free condition at the boundary $\partial_{\mathbf{n}} \phi|_{\partial\Omega} = 0$ and $\partial_{\mathbf{n}} \Delta \phi|_{\partial\Omega} = 0$ is chosen to ensure that the boundary integrals resulting during the integration by parts vanish, where $\mathbf{n}$ is the outward normal on the boundary.

There has been a great number of works contributed to the investigation of numerical approximations for the solution of the phase field models, for instance, the so-called convex splitting techniques [2, 26, 30, 31] and the stabilized semi-implicit methods [25, 27, 32]. More recently, there are two novel strategies that are used to design second-order, unconditionally energy stable numerical schemes to solve the phase field models: the invariant energy quadratization (IEQ) method [33] and the scalar auxiliary variable (SAV) approach [3]. The latter is inspired by the former and leads to numerical schemes in which only decoupled equations with constant coefficients need to be solved at each time-step. The common goal of IEQ and SAV methods is to transform the primitive system into a new equivalent system with a quadratic energy functional and the corresponding modified energy dissipation property. Rigorous analysis and comparisons between IEQ and SAV might be out of this article's scope; we refer to [3, 7, 33] for more details.

In comparison with the bright achievement of classical phase field models, there are many researches on building fractional phase field models to better model the anomalously diffusive effects. For instance, the time, space, and time-space fractional Allen–Cahn equations were suggested [9, 13, 20, 34] to accurately describe anomalous diffusion problems. Li, Wang, and yang [13] investigated a space-time fractional Allen–Cahn phase field model that describes the transport of the fluid mixture of two immiscible fluid phases. They concluded that the alternative model could provide more accurate description of anomalous diffusion processes and sharper interfaces than the classical model. Hou, Tang, and Yang [9] showed that the space-fractional Allen–Cahn equation could be viewed as an L^2 gradient flow for the fractional analog version of the Ginzburg–Landau free energy function. Also, they proved that the space-fractional Allen–Cahn equation preserves the energy dissipation property and the maximum principle. The first theoretical contribution regarding the energy dissipation property of the time-fractional phase models was made by Tang, Yu, and Zhou [28]. They proved that the time-fractional phase field models indeed admit an energy dissipation law of an integral type. Meanwhile, they applied the uniform L1

formula to construct a class of finite difference schemes, which can inherit the theoretical energy dissipation property in the discrete levels. Along the numerical front, Zhao et al. [20, 34] studied a series of the time-fractional phase field models numerically, covering the time-fractional Cahn–Hilliard equation with different types of variable mobilities and time-fractional MBE model with and without slope selection. The considerable numerical evidences indicate that the effective free energy and roughness of the time-fractional phase field models during coarsening obey the similar power scaling laws as the integer-order ones, where the power is linearly proportional to the fractional index α. In other words, the main difference between the time-fractional phase field models and integer-order ones lie in the time scales of coarsening.

The multiscale nature of time-fractional phase field models prompts us to construct reliable time-stepping methods on general nonuniform time meshes. In this paper, nonuniform time-stepping schemes are investigated for the time-fractional MBE model [28],

$$\partial_t^\alpha \phi = -M\left(\varepsilon^2 \Delta^2 \phi - \nabla \cdot f\left(\nabla \phi\right)\right), \tag{1.4}$$

where ∂_t^α in (1.4) denotes the Caputo fractional derivative of order α with respect to t,

$$(\partial_t^\alpha v)(t) := (\mathcal{I}_t^{1-\alpha} v')(t) = \int_0^t \omega_{1-\alpha}(t-s) v'(s)\,\mathrm{d}s, \quad 0<\alpha<1, \tag{1.5}$$

involving the fractional Riemann–Liouville integral $\mathcal{I}_t^\beta$ of order $\beta > 0$, that is,

$$(\mathcal{I}_t^\beta v)(t) := \int_0^t \omega_\beta(t-s) v(s)\,\mathrm{d}s, \quad \text{where} \quad \omega_\beta(t) := t^{\beta-1}/\Gamma(\beta).$$

Specifically, in comparison to the decay property (1.3) of the classical MBE model, the energy dissipation law of the time-fractional MBE model (1.4) (see also [28]), is given by

$$E\left[\phi(T)\right] - E\left[\phi(0)\right] = -\frac{1}{M}\int_\Omega \int_0^T \left(\partial_t^\alpha \phi\right)\partial_t \phi \,\mathrm{d}t\,\mathrm{d}\mathbf{x} \leqslant 0. \tag{1.6}$$

To our knowledge, there are few results in the literatures on the discrete energy dissipation laws of numerical approaches for the time-fractional phase field models, especially on nonuniform time meshes. One of our interests in this paper is to build nonuniform time-stepping methods preserving the energy dissipation law of the problem (1.4) in the discrete time levels.

Consider the nonuniform time levels $0 = t_0 < t_1 < \cdots < t_{k-1} < t_k < \cdots < t_N = T$ with the time-step sizes $\tau_k := t_k - t_{k-1}$ for $1 \leqslant k \leqslant N$, and denote the maximum time-step size $\tau := \max_{1\leqslant k\leqslant N} \tau_k$. Also, let the local time-step ratio $\rho_k := \tau_k/\tau_{k+1}$. Given a grid function $\{v^k\}$, put $\nabla_\tau v^k := v^k - v^{k-1}$, $\partial_\tau v^{k-\frac{1}{2}} := \nabla_\tau v^k/\tau_k$, and $v^{k-\frac{1}{2}} := (v^k + v^{k-1})/2$ for $k \geq 1$. Always, let $(\Pi_{1,k} v)(t)$ denote the linear interpolant of a function $v(t)$ at two nodes t_{k-1} and t_k, and define a piecewise linear approximation

$$\Pi_1 v := \Pi_{1,k} v \quad \text{so that} \quad (\Pi_1 v)'(t) = \partial_\tau v^{k-\frac{1}{2}} \quad \text{for } t_{k-1} < t \leqslant t_k \text{ and } k \geq 1.$$

As an essential mathematical feature of linear and nonlinear subdiffusion problems including the time-fractional MBE model (1.4), the solution always lacks the smoothness near the initial time, although it would be smooth away from $t = 0$; see [11, 12].

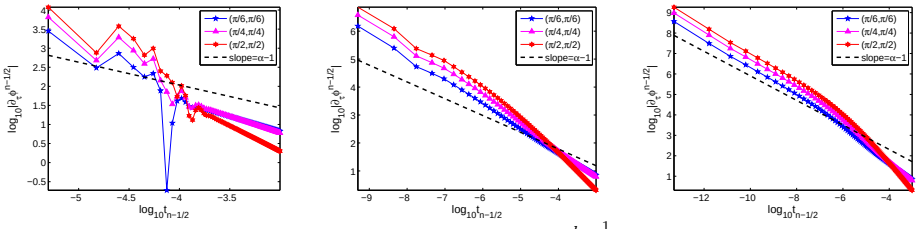

FIG. 1. *The log-log plot of the difference quotient* $\partial_\tau \phi^{k-\frac{1}{2}}$ *versus time for problem* (1.4) *with fractional order* $\alpha = 0.4$ *and* $\gamma = 1, 3, 5$ *(from left to right), respectively.*

Actually, in any numerical methods for solving time-fractional diffusion equations, a key consideration is the initial singularity of solution; see the recent works [14, 16, 18]. More directly, we apply a new L1-type formula to the time-fractional problem (1.4); see more details in subsection 3.1 and Example 4.3. Figure 1 plots the discrete time derivative $\partial_\tau \phi^{k-\frac{1}{2}}$ near $t = 0$ on the graded mesh $t_k = (k/N)^\gamma$ when $\alpha = 0.4$. The numerical results of Figure 1 suggest that

$$\log |\phi_t(\mathbf{x}, t)| \approx (\alpha - 1) \log(t) + C(\mathbf{x}) \quad \text{as } t \to 0.$$

It says that the solution possesses weakly singularity like $\phi_t = O(t^{\alpha-1})$ near initial time, which can be alleviated by using the graded meshes. Thus, the second interest of this paper is to resolve the essentially weak singularity in (1.4) by refining time mesh. Actually, we will show that the graded mesh can recover the optimal time accuracy when the solution ϕ is nonsmooth near $t = 0$.

In the next section, we reformulate the time-fractional MBE model (1.4) by using SAV technique, which provides an elegant platform for constructing energy stable schemes. Although the L1 formula was applied in [28] to treat the time-fractional phase field models and the discrete energy decay laws were also established on uniform time mesh, we are not able to exploit any discrete energy dissipation laws under the adaptive time-steps and leave it as an open problem (see Remark 1). This open problem guides us to develop a novel numerical Caputo derivative (3.6), called L1$^+$ formula, which preserves inherently the positive semidefinite property of integral kernel; see (3.8). This new formula is as simple as the classical L1 formula because it is also constructed by the piecewise linear interpolation; however, it can achieve second-order accurate for all fractional orders $\alpha \in (0, 1)$ and substantially improves the accuracy of L1 formula, especially when the fractional order $\alpha \to 1$. Applying the new formula to the time-fractional MBE model (1.4), we obtain two linearized Crank–Nicolson schemes, (3.9)–(3.10) and (3.11)–(3.12), respectively. Thus it is straightforward to confirm that both of them preserve the discrete energy dissipation law well (see Theorems 3.1 and 3.2) so that they are unconditionally stable in the energy norm. Extensive numerical experiments are carried out in section 4 to show the effectiveness of our numerical approaches and to support our analysis.

In summary, the main contributions of this paper for the time-fractional MBE model (1.4) are the following: suggest a simple L1$^+$ formula of Caputo derivative having second-order accuracy for any fractional order $\alpha \in (0, 1)$ and apply it to build two linearized Crank–Nicolson schemes preserving the discrete energy dissipation law for the time-fractional MBE model (1.4).

2. Model reformulation using the SAV strategy. For simplicity, denote the time-fractional MBE model (1.4) with and without slope selection as "Slope Model"

and "No-Slope Model," respectively. Additionally, boundary conditions are set to be periodic so as not to complicate the analysis with unwanted details. We then reformulate the time-fractional MBE models into the equivalent PDE systems by borrowing the ideas from the IEQ and SAV methods [3, 7, 33].

2.1. The Slope Model and its equivalent system. We introduce a scalar auxiliary function $u(t)$ in term of original variable ϕ given by

$$u(t) = u[\phi] = \sqrt{\int_\Omega \frac{1}{4}\left(|\nabla\phi|^2 - 1 - \beta\right)^2 \mathrm{d}\mathbf{x} + C_0},$$

where $C_0 > 0$ is a constant that ensures the radicand positive. Compared with those in [3, 33], the SAV $u(t)$ adds an artificial parameter $\beta > 0$ to regularize the numerical approach. As a consequence, the free energy of the Slope Model is transformed into a quadratic form

$$E_1[\phi, u] = \int_\Omega \left(\frac{\varepsilon^2}{2}|\Delta\phi|^2 + \frac{\beta}{2}|\nabla\phi|^2\right)\mathrm{d}\mathbf{x} + u^2 - \left(\frac{\beta}{2} + \frac{\beta^2}{4}\right)|\Omega| - C_0. \tag{2.1}$$

Correspondingly, the Slope Model can be reformulated to the following equivalent form:

$$\partial_t^\alpha \phi = -M\left(\varepsilon^2\Delta^2\phi - \beta\Delta\phi - U[\phi]\, u\right), \tag{2.2}$$

$$u_t = -\frac{1}{2}\int_\Omega U[\phi]\,\partial_t\phi\,\mathrm{d}\mathbf{x}, \tag{2.3}$$

where the expression of notation $U[\phi]$ is given by

$$U[\phi] = \frac{\nabla\cdot\left(\left(|\nabla\phi|^2 - 1 - \beta\right)\nabla\phi\right)}{\sqrt{\int_\Omega \frac{1}{4}\left(|\nabla\phi|^2 - 1 - \beta\right)^2 \mathrm{d}\mathbf{x} + C_0}}.$$

We should note that the new system is subjected to the initial conditions

$$\phi(\mathbf{x}, 0) = \phi_0(\mathbf{x}) \quad \text{and} \quad u(0) = u[\phi_0],$$

and the boundary conditions are same as the primitive model. By taking the L^2 inner product of (2.2) with $\partial_t\phi$, of (2.3) with u, and then making time integrations on both sides, we see the equivalent system preserves the modified energy dissipation law

$$E_1[\phi(T), u(T)] - E_1[\phi(0), u(0)] = -\frac{1}{M}\int_\Omega\int_0^T \left(\partial_t^\alpha\phi\right)\partial_t\phi\,\mathrm{d}t\,\mathrm{d}\mathbf{x} \leqslant 0. \tag{2.4}$$

The nonpositive of the right part of above equality is determined by [28, Corollary 2.1].

2.2. The No-Slope Model and its equivalent system. For the No-Slope Model, we introduce a scalar auxiliary function $v(t)$ in term of original variable ϕ as follows:

$$v(t) = v[\phi] = \sqrt{\int_\Omega \left(\frac{1}{2}\ln\left(1 + |\nabla\phi|^2\right) + \frac{\beta}{2}|\nabla\phi|^2\right)\mathrm{d}\mathbf{x} + C_0}, \tag{2.5}$$

where β and C_0 are similar to the previous ones. Therefore, the free energy of the No-Slope Model could be rewritten into

$$E_2[\phi, v] = \int_\Omega \left(\frac{\varepsilon^2}{2} |\Delta\phi|^2 + \frac{\beta}{2} |\nabla\phi|^2 \right) \mathrm{d}\mathbf{x} - v^2 + C_0. \tag{2.6}$$

We then could rewrite the No-Slope Model as an equivalent form

$$\partial_t^\alpha \phi = -M \left(\varepsilon^2 \Delta^2 \phi - \beta \Delta\phi + V[\phi] v \right), \tag{2.7}$$

$$v_t = -\frac{1}{2} \int_\Omega V[\phi] \partial_t \phi \, \mathrm{d}\mathbf{x}, \tag{2.8}$$

in which

$$V[\phi] = \frac{\nabla \cdot \left(\left(\frac{1}{1+|\nabla\phi|^2} + \beta \right) \nabla\phi \right)}{\sqrt{\int_\Omega \left(\frac{1}{2} \ln\left(1 + |\nabla\phi|^2\right) + \frac{\beta}{2} |\nabla\phi|^2 \right) \mathrm{d}\mathbf{x} + C_0}},$$

with the following initial conditions:

$$\phi(\mathbf{x}, 0) = \phi_0(\mathbf{x}) \quad \text{and} \quad v(0) = v[\phi_0].$$

Similarly, the new system admits the following modified energy dissipation law:

$$E_2[\phi(T), v(T)] - E_2[\phi(0), v(0)] = -\frac{1}{M} \int_\Omega \int_0^T \left(\partial_t^\alpha \phi \right) \partial_t \phi \, \mathrm{d}t \, \mathrm{d}\mathbf{x} \leqslant 0. \tag{2.9}$$

We note that the transformed systems (2.2)–(2.3) and (2.7)–(2.8) are equivalent to their original systems in the continuous sense, respectively. The corresponding modified energies are also equivalent to the original ones. We will focus on developing accurate numerical methods preserving the modified energies of the reformulated models in what follows.

3. Novel L1$^+$ formula and Crank–Nicolson SAV schemes. The well-known L1 formula of Caputo derivative is given by

$$(\partial_\tau^\alpha v)^n := \int_{t_0}^{t_n} \omega_{1-\alpha}(t_n - s)(\Pi_1 v)'(s) \, \mathrm{d}s = \sum_{k=1}^{n} a_{n-k}^{(n)} \nabla_\tau v^k, \tag{3.1}$$

where the corresponding discrete convolution kernels $a_{n-k}^{(n)}$ are defined by

$$a_{n-k}^{(n)} := \frac{1}{\tau_k} \int_{t_{k-1}}^{t_k} \omega_{1-\alpha}(t_n - s) \, \mathrm{d}s \quad \text{for } 1 \leqslant k \leqslant n. \tag{3.2}$$

Obviously, the discrete L1 kernels $a_{n-k}^{(n)}$ are positive and decreasing (see also [14, 18]):

$$a_{n-k}^{(n)} > 0 \quad \text{and} \quad a_{n-k-1}^{(n)} > a_{n-k}^{(n)} \quad \text{for } 1 \leqslant k \leqslant n-1. \tag{3.3}$$

Based on the above L1 formula on uniform time mesh, a linearized scheme by using the stabilized technique via a stabilized term $S(\Delta\phi^n - \Delta\phi^{n-1})$ for a properly large scalar parameter $S > 0$ is presented. We refer to [28] for more details. The resulting stabilized semi-implicit scheme for the problem (1.4) without slope selection reads

$$(\partial_\tau^\alpha \phi)^n = -M \left(\varepsilon^2 \Delta^2 \phi^n - \nabla \cdot f\left(\nabla \phi^{n-1} \right) \right) + S(\Delta\phi^n - \Delta\phi^{n-1}). \tag{3.4}$$

Let us mention that, when the time mesh is uniform such that the discrete L1 kernels

$$a_{n-k}^{(n)} = a_{n-k} = \frac{1}{\tau^\alpha}\left[\omega_{2-\alpha}(n-k+1) - \omega_{2-\alpha}(n-k)\right] \quad \text{for } 1 \leqslant k \leqslant n,$$

the semi-implicit scheme (3.4) preserves a discrete energy dissipation law; see more details in [28, Theorem 3.3]. As seen, the proof of discrete version of energy dissipation law (1.6) relies on the positive semidefinite property of a discrete quadratic form $\sum_{k=1}^{n} q_k \sum_{j=1}^{k} a_{k-j} q_j \geq 0$.

Remark 1. It seems rather difficult to extend the positive semidefinite property to a general class of nonuniform meshes. More precisely, we are not able to verify the positive semidefinite property of the following quadratic form (by taking $q_k = \nabla_\tau \phi^k$):

$$\sum_{k=1}^{n} \nabla_\tau \phi^k (\partial_\tau^\alpha \phi)^k = \sum_{k=1}^{n} q_k \sum_{j=1}^{k} a_{k-j}^{(k)} q_j \geq 0.$$

The open problem in Remark 1 motivates us to design a novel discrete Caputo formula such that it naturally preserves the energy dissipation property in the discrete sense for the time-fractional MBE model. Alternatively, the novel discrete Caputo formula should inherit the positive semidefinite property of a quadratic form in Remark 1.

Fortunately, as pointed out early in [22, 23], we know that the weakly singular kernel $\omega_{1-\alpha}$ is positive semidefinite, that is,

$$\begin{aligned} \mathcal{I}_t^1 (q\, \mathcal{I}_t^{1-\alpha} q)(t) &= \int_0^t q(\mu)\, \mathrm{d}\mu \int_0^\mu \omega_{1-\alpha}(\mu - s) q(s)\, \mathrm{d}s \\ &= \frac{1}{2} \int_0^t \int_0^t \omega_{1-\alpha}(|\mu - s|) q(\mu) q(s)\, \mathrm{d}\mu\, \mathrm{d}s \geq 0 \end{aligned} \tag{3.5}$$

for $t > 0$ and any $q \in C[0,T]$. Very recently, Tang, Yu, and Zhou [28, Lemma 2.1 and Corollary 2.1] showed that this property (3.5) holds if $q \in L^p(0,T)$ with $p \geq \frac{2}{2-\alpha}$ for $\alpha \in (0,1)$. This result permits some weakly singular functions like $q = O(t^{\alpha-1})$ for $\alpha \in (0,1)$ to ensure the positive semidefiniteness. We will see that a discrete counterpart of (3.5) yields a discrete Caputo approximation preserving the desired energy dissipation property when it is applied to time-fractional MBE models.

3.1. The L1$^+$ formula. The L1$^+$ formula for the Caputo derivative (1.5) is defined at time $t = t_{n-\frac{1}{2}}$ as follows:

$$(\partial_\tau^\alpha v)^{n-\frac{1}{2}} := \frac{1}{\tau_n} \int_{t_{n-1}}^{t_n} \int_0^t \omega_{1-\alpha}(t-s)(\Pi_1 v)'(s)\, \mathrm{d}s\, \mathrm{d}t = \sum_{k=1}^{n} \bar{a}_{n-k}^{(n)} \nabla_\tau v^k \quad \text{for } n \geq 1, \tag{3.6}$$

where the discrete convolution kernels $\bar{a}_{n-k}^{(n)}$ are defined by

$$\bar{a}_{n-k}^{(n)} := \frac{1}{\tau_n \tau_k} \int_{t_{n-1}}^{t_n} \int_{t_{k-1}}^{\min\{t, t_k\}} \omega_{1-\alpha}(t-s)\, \mathrm{d}s\, \mathrm{d}t \quad \text{for } 1 \leqslant k \leqslant n. \tag{3.7}$$

Evidently, the naturally nonuniform L1$^+$ approximation

$$(\partial_\tau^\alpha v)^{n-\frac{1}{2}} \approx \frac{1}{\tau_n} \int_{t_{n-1}}^{t_n} (\partial_t^\alpha v)(t)\, \mathrm{d}t$$

ensures the positive semidefinite property (3.5) by taking $q = (\Pi_1 v)'$, that is,

$$\begin{aligned}\sum_{k=1}^{n} \nabla_\tau v^k (\partial_\tau^\alpha v)^{k-\frac{1}{2}} &= \sum_{k=1}^{n} \tau_k (\Pi_{1,k} v)'(\partial_\tau^\alpha v)^{k-\frac{1}{2}} \\ &= \int_{t_0}^{t_n} (\Pi_1 v)'(t) \int_0^t \omega_{1-\alpha}(t-s)(\Pi_1 v)'(s)\,\mathrm{d}s\,\mathrm{d}t \\ &= \mathcal{I}_t^1 \Big[(\Pi_1 v)' \mathcal{I}_t^{1-\alpha} (\Pi_1 v)' \Big](t_n) \geq 0 \quad \text{for } n \geq 1, \end{aligned} \tag{3.8}$$

where [28, Corollary 2.1] has been used. Thus the definition (3.7) and the arbitrariness of function v yield the following result.

LEMMA 3.1. *The discrete convolution kernels $\bar{a}_{n-k}^{(n)}$ in (3.7) are positive, and for any real sequence $\{q_k\}_{k=1}^n$ with n entries, it holds that*

$$\sum_{k=1}^{n} q_k \sum_{j=1}^{k} \bar{a}_{k-j}^{(k)} q_j \geq 0 \quad \textit{for } n \geq 1.$$

Before applying the L1$^+$ formula (3.6) to the time-fractional MBE model (1.4), we consider a simple fractional ODE problem $\partial_t^\alpha y(t) = f(t)$ for $0 < t < 1$. Choosing a smooth solution $y = \omega_{1+\sigma}(t)$ with the regularity parameter $\sigma = 2.5$, we run a Crank–Nicolson-type scheme $(\partial_\tau^\alpha y)^{n-\frac{1}{2}} = f(t_{n-\frac{1}{2}})$ with uniform step $\tau_k = \tau$ until $T = 1$. The discrete l^∞ norm errors $e(N) = \max_{1\leqslant n\leqslant N} |y(t_n) - y^n|$ are listed in Table 1. It seems that the numerical accuracy of (3.6) is second-order accurate for any fractional order $\alpha \in (0, 1)$. If the solution has an initial singularity, the L1$^+$ formula (3.6) can also achieve second-order accuracy by properly refining the mesh near $t = 0$; see more tests in Example 4.1.

Remark 2. The complete consistency analysis of the $L1^+$ formula on arbitrary time meshes will be considered in a separate article. In fact, the error analysis would be lengthy and complex, even on the uniform time mesh. However, the $L1^+$ formula is formally second-order accurate provided that the solution is smooth. Typically, there is no error for $v = 1$ and $v = t$. Considering $v = t^2$ on the uniform mesh, we have

$$\begin{aligned}\Upsilon^{n-\frac{1}{2}} :=& \frac{1}{\tau} \sum_{k=1}^{n-1} \int_{t_{n-1}}^{t_n} \int_{t_{k-1}}^{t_k} \omega_{1-\alpha}(t-s)(\widetilde{\Pi_{1,k}} v)'(s)\,\mathrm{d}s\,\mathrm{d}t \\ &+ \frac{1}{\tau} \int_{t_{n-1}}^{t_n} \int_{t_{n-1}}^{t} \omega_{1-\alpha}(t-s)(\widetilde{\Pi_{1,n}} v)'(s)\,\mathrm{d}s\,\mathrm{d}t \triangleq \sum_{k=1}^{n-1} \Upsilon_k^{n-\frac{1}{2}} + \Upsilon_n^{n-\frac{1}{2}}, \end{aligned}$$

where $(\widetilde{\Pi_{1,k}} v)(t) = v(t) - (\Pi_{1,k} v)(t)$ denotes the interpolation error. A careful calculation yields

TABLE 1
Numerical accuracy of $L1^+$ formula (3.6) with $\sigma = 2.5$.

N	$\alpha = 0.1$		$\alpha = 0.5$		$\alpha = 0.9$	
	$e(N)$	Order	$e(N)$	Order	$e(N)$	Order
64	3.44e-05	–	3.39e-05	–	2.25e-05	–
128	8.61e-06	2.00	8.51e-06	1.99	5.83e-06	1.95
256	2.15e-06	2.00	3.13e-06	1.99	1.51e-06	1.95
512	5.38e-07	2.00	5.35e-07	2.00	3.88e-07	1.96

$$\begin{aligned}\Upsilon_k^{n-\frac{1}{2}} &= \frac{2}{\tau}\int_{t_{n-1}}^{t_n}\int_{t_{k-1}}^{t_k}\omega_{1-\alpha}(t-s)(s-t_{k-\frac{1}{2}})\,\mathrm{d}s\,\mathrm{d}t\\ &= \frac{2}{\tau}\left[\omega_{4-\alpha}(t_{n-k+1})-\omega_{4-\alpha}(t_{n-k})\right]-\frac{2}{\tau}\left[\omega_{4-\alpha}(t_{n-k})-\omega_{4-\alpha}(t_{n-k-1})\right]\\ &\quad-\left[\omega_{3-\alpha}(t_{n-k+1})-\omega_{3-\alpha}(t_{n-k})\right]-\left[\omega_{3-\alpha}(t_{n-k})-\omega_{3-\alpha}(t_{n-k-1})\right]\end{aligned}$$

for $1\le k\le n-1$ and

$$\Upsilon_n^{n-\frac{1}{2}} = \frac{2}{\tau}\int_{t_{n-1}}^{t_n}\int_{t_{n-1}}^{t}\omega_{1-\alpha}(t-s)(s-t_{n-\frac{1}{2}})\,\mathrm{d}s\,\mathrm{d}t = \frac{2}{\tau}\omega_{4-\alpha}(\tau)-\omega_{3-\alpha}(\tau).$$

Taking $n=1$ gives $\left|\Upsilon^{\frac{1}{2}}\right| = \left|\Upsilon_1^{\frac{1}{2}}\right| \le \frac{1-\alpha}{\Gamma(4-\alpha)}\tau^{2-\alpha}$. By using [16, Lemma 2.1], it follows that

$$\begin{aligned}\Upsilon^{n-\frac{1}{2}} &= \sum_{k=1}^{n}\Upsilon_k^{n-\frac{1}{2}} = \frac{2}{\tau}\left[\omega_{4-\alpha}(t_n)-\omega_{4-\alpha}(t_{n-1})\right]-\left[\omega_{3-\alpha}(t_n)+\omega_{3-\alpha}(t_{n-1})\right]\\ &= \frac{2}{\tau}\int_{t_{n-1}}^{t_n}\left[\omega_{3-\alpha}(t)-\left(\Pi_{1,n}\omega_{3-\alpha}\right)(t)\right]\,\mathrm{d}t\\ &= -\frac{1}{\tau}\int_{t_{n-1}}^{t_n}(t_n-t)(t-t_{n-1})\omega_{1-\alpha}(t)\,\mathrm{d}t.\end{aligned}$$

Thus we have $\left|\Upsilon^{n-\frac{1}{2}}\right| \le \frac{1}{6}\omega_{1-\alpha}(t_{n-1})\tau^2$ for $n\ge 2$.

3.2. Crank–Nicolson SAV schemes preserving energy dissipation. In what follows, we are concerned only with the time discretization of the equivalent systems, while the spatial approximations can be diverse, for example, as finite difference, finite element, or spectral methods. Integrating (2.2)–(2.3) from $t=t_{n-1}$ to t_n, respectively, leads to

$$\begin{aligned}\frac{1}{\tau_n}\int_{t_{n-1}}^{t_n}\partial_t^\alpha\phi\,\mathrm{d}t &= -\frac{M}{\tau_n}\int_{t_{n-1}}^{t_n}\left(\varepsilon^2\Delta^2\phi-\beta\Delta\phi-U\left[\phi\right]u\right)\,\mathrm{d}t,\\ \frac{1}{\tau_n}\int_{t_{n-1}}^{t_n}u_t\,\mathrm{d}t &= -\frac{1}{2\tau_n}\int_{t_{n-1}}^{t_n}\int_\Omega U\left[\phi\right]\partial_t\phi\,\mathrm{d}\mathbf{x}\,\mathrm{d}t.\end{aligned}$$

Applying the $\mathrm{L1}^+$ formula (3.6), the trapezoidal formula, we have the following Crank–Nicolson SAV (CN-SAV) time-stepping scheme for the Slope Model (2.2)–(2.3):

$$(\partial_\tau^\alpha\phi)^{n-\frac{1}{2}} = -M\left(\varepsilon^2\Delta^2\phi^{n-\frac{1}{2}}-\beta\Delta\phi^{n-\frac{1}{2}}-U\big[\hat{\phi}^{n-\frac{1}{2}}\big]u^{n-\frac{1}{2}}\right), \tag{3.9}$$

$$\partial_\tau u^{n-\frac{1}{2}} = -\frac{1}{2}\int_\Omega U\big[\hat{\phi}^{n-\frac{1}{2}}\big]\partial_\tau\phi^{n-\frac{1}{2}}\,\mathrm{d}\mathbf{x}, \tag{3.10}$$

where $\hat{\phi}^{n-\frac{1}{2}} := \phi^{n-1}+\nabla_\tau\phi^{n-1}/(2\rho_{n-1})$ is the local extrapolation.

Note that the construction of $\mathrm{L1}^+$ formula (3.6) implies that the above CN-SAV scheme (3.9)–(3.10) is naturally suitable for a general class of nonuniform meshes. Moreover, the next result shows that it is unconditionally energy stable.

THEOREM 3.1. *The CN-SAV scheme* (3.9)–(3.10) *preserves the modified energy dissipation law,*

$$E_1\left[\phi^n,u^n\right]-E_1\left[\phi^0,u^0\right]\leqslant 0 \quad \textit{for} \quad 1\leqslant n\leqslant N,$$

such that it is unconditionally stable, where

$$E_1\left[\phi^n, u^n\right] = \int_\Omega \left(\frac{\varepsilon^2}{2}\left|\Delta\phi^n\right|^2 + \frac{\beta}{2}\left|\nabla\phi^n\right|^2\right) \mathrm{d}\mathbf{x} + \left(u^n\right)^2 - C_0.$$

Proof. Taking the inner product of (3.9) and (3.10) with $\nabla_\tau\phi^n/M$ and $2\tau_n u^{n-\frac{1}{2}}$, respectively, and adding the resulting two identities, we obtain

$$-\frac{1}{M}\left(\left(\partial_\tau^\alpha\phi\right)^{n-\frac{1}{2}}, \nabla_\tau\phi^n\right) = \left(\varepsilon^2\Delta^2\phi^{n-\frac{1}{2}} - \beta\Delta\phi^{n-\frac{1}{2}}, \nabla_\tau\phi^n\right) + \left(u^n\right)^2 - \left(u^{n-1}\right)^2,$$

which implies that

$$E_1\left[\phi^k, u^k\right] - E_1\left[\phi^{k-1}, u^{k-1}\right] = -\frac{1}{M}\left(\left(\partial_\tau^\alpha\phi\right)^{k-\frac{1}{2}}, \nabla_\tau\phi^k\right) \quad \text{for } 1 \leqslant k \leqslant n.$$

By summing the superscript k from 1 to n, we apply the property (3.8) to derive that

$$E_1\left[\phi^n, u^n\right] - E_1\left[\phi^0, u^0\right] = -\frac{1}{M}\int_\Omega \mathcal{I}_t^1\left[(\Pi_1\phi)'\mathcal{I}_t^{1-\alpha}(\Pi_1\phi)'\right](t_n)\,\mathrm{d}\mathbf{x} \leqslant 0$$

for $1 \leqslant n \leqslant N$. This completes the proof. ∎

Analogously, for the No-Slope Model (2.7)–(2.8), we present the following CN-SAV time-stepping scheme:

$$\left(\partial_\tau^\alpha\phi\right)^{n-\frac{1}{2}} = -M\left(\varepsilon^2\Delta^2\phi^{n-\frac{1}{2}} - \beta\Delta\phi^{n-\frac{1}{2}} + V\left[\hat{\phi}^{n-\frac{1}{2}}\right]v^{n-\frac{1}{2}}\right), \tag{3.11}$$

$$\partial_\tau v^{n-\frac{1}{2}} = -\frac{1}{2}\int_\Omega V\left[\hat{\phi}^{n-\frac{1}{2}}\right]\partial_\tau\phi^{n-\frac{1}{2}}\,\mathrm{d}\mathbf{x}. \tag{3.12}$$

For the above numerical scheme, we shall only state the energy dissipation law below, as their proofs are essentially the same as Theorem 3.1.

THEOREM 3.2. *The CN-SAV scheme* (3.11)–(3.12) *satisfies the following modified energy dissipation law:*

$$E_2\left[\phi^n, v^n\right] - E_2\left[\phi^0, v^0\right] \leqslant 0,$$

in which

$$E_2\left[\phi^n, v^n\right] = \int_\Omega \left(\frac{\varepsilon^2}{2}\left|\Delta\phi^n\right|^2 + \frac{\beta}{2}\left|\nabla\phi^n\right|^2\right) \mathrm{d}\mathbf{x} - \left(v^n\right)^2 + C_0.$$

Remark 3. Although our auxiliary variable $v[\phi]$ cannot guarantee a lower bound of the modified energy $E_2[\phi, v]$ in the discrete levels, the techniques used in [2, 30] provide a new perspective to introduce new auxiliary variable, which may guarantee a lower bound of the modified energy. Noticing the inequality

$$-\frac{1}{2}\ln(1+|v|^2) \geq -\frac{1}{2}\left(\theta\left|v\right|^2 - \ln(\theta) + \theta - 1\right) \quad \forall\, 0 < \theta \leq 1,$$

taking $\theta = \frac{4\pi^2\varepsilon^2}{L^2}$, and using the elliptic regularity estimate

$$\left\|\Delta\phi\right\|^2 \geq \frac{4\pi^2}{L^2}\left\|\nabla\phi\right\|^2 \quad \text{for } \forall\,\phi \in H^2_{per}(\Omega) \text{ and } \Omega = (0, L)^2,$$

a lower bound of the original energy of the classical (integer-order) MBE without slope selection has been established in [2],

$$E[\phi] \geq \frac{L^2}{2}\left(\ln\left(\frac{4\pi^2\varepsilon^2}{L^2}\right) - \frac{4\pi^2\varepsilon^2}{L^2} + 1\right).$$

Remark 4. The modified energy dissipation laws (2.4) and (2.9) are equivalent to the original energy dissipation laws in continuous sense, respectively, but not for the discrete levels. In other words, the CN-SAV schemes (3.9)–(3.10) and (3.11)–(3.12) may not preserve the discrete counterpart of the original energy dissipative property (1.6). However, the proposed schemes conserve the modified energy dissipation laws and thus are structure-preserving in some senses, which allows them to perform good numerical behavior.

3.3. Further notes on L1$^+$ formula.

Remark 5 (multiterm and distributed time-fractional problems). As seen in Table 1 and more tests in the next section, the accuracy of the $L1^+$ formula (3.6) is dependent on the regularity of solution but would be independent of the fractional order $\alpha \in (0,1)$. It is quite different from some exiting numerical approaches, such as $L1$, Alikhanov [1, 19], and BDF2-like formulas [5, 15, 21], of which the consistency errors are dependent on the fractional order α. This feature is attractive for further applications in developing second-order approximations for multiterm and distributed-order fractional diffusion equations. For an example, consider a simple multiterm fractional diffusion problem,

$$\sum_{i=1}^{m} w_i \, \partial_t^{\alpha_i} u = \Delta u + f,$$

where $0 < \alpha_i < 1$ for $1 \leqslant i \leqslant m$, and w_i are the corresponding weights. One can construct the following second-order Crank–Nicolson-type time-stepping scheme:

$$\sum_{\nu=1}^{m} w_i (\partial_\tau^{\alpha_i} u)^{n-\frac{1}{2}} = \Delta u^{n-\frac{1}{2}} + f^{n-\frac{1}{2}} \quad \text{for } 1 \leqslant n \leqslant N.$$

Obviously, the $L1^+$ formula (3.6) would be also useful in approximating the distributed-order Caputo derivative since it can be approximated by certain multiterm fractional derivatives via some proper quadrature rule; see [15].

The suggested L1$^+$ formula (3.6) seems very promising in further applications for other time-fractional field phase models and other time-fractional differential equations. We thus note that the rigorous theoretical analysis on consistency, stability, and convergence very important, especially on a general class of nonuniform meshes.

However, the established stability and convergence theory [14, 16, 17, 18] for variable-step L1 and L1-2$_\sigma$ (Alikhanov) formulas cannot be applied to the L1$^+$ formula directly because the discrete convolution kernels $\bar{a}_{n-k}^{(n)}$ in (3.7) do not have the uniform monotonicity like (3.2). Actually, the definition (3.7) and the integral mean-value theorem yield the following result.

LEMMA 3.2. *The positive discrete kernels* $\bar{a}_{n-k}^{(n)}$ *in* (3.7) *fulfill*

$$\bar{a}_0^{(n)} = \frac{1}{\Gamma(3-\alpha)\tau_n^\alpha}, \quad \bar{a}_1^{(n)} > \bar{a}_2^{(n)} > \cdots > \bar{a}_{n-1}^{(n)} > 0 \quad \textit{for } n \geq 2.$$

Notwithstanding, it ought to be emphasized that

$$\bar{a}_0^{(n)} - \bar{a}_1^{(n)} = \frac{1}{\Gamma(3-\alpha)\tau_n^\alpha \rho_{n-1}} \left(1 + \rho_{n-1} + \rho_{n-1}^{2-\alpha} - (1+\rho_{n-1})^{2-\alpha}\right).$$

It is easily seen that $\bar{a}_0^{(n)} < \bar{a}_1^{(n)}$ as $\alpha \to 0$ and $\bar{a}_0^{(n)} > \bar{a}_1^{(n)}$ as $\alpha \to 1$; So the value of $\bar{a}_0^{(n)} - \bar{a}_1^{(n)}$ may change the sign when the fractional order α varies over

$(0,1)$. At the same time, this situation is no worse than the case in the BDF2-like formulas [15] in which the second kernel would be negative when $\alpha \to 1$; see more details and a potential remedy technique in [17, Remark 6]. The theoretical investigations, including the consistency, stability, and convergence, of nonuniform L1$^+$ formula (3.6), will be addressed in a separate report.

4. Numerical algorithms and examples.

4.1. A fast version of L1$^+$ formula. It is evident that the approximations (3.1) or (3.6) are prohibitively expensive for long-time simulations due to the long-time memory. In order to reduce the computational cost and storage requirements, we apply the sum-of-exponentials (SOE) technique to speed up the evaluation of the L1$^+$ formula. A core result is to approximate the kernel function $\omega_{1-\alpha}(t)$ efficiently on the interval $[\Delta t, T]$; see [10, Theorem 2.1].

LEMMA 4.1. *For the given $\alpha \in (0,1)$, an absolute tolerance error $\epsilon \ll 1$, a cutoff time $\Delta t > 0$, and a final time T, there exists a positive integer N_q, positive quadrature nodes θ^ℓ, and corresponding positive weights ϖ^ℓ $(1 \leqslant \ell \leqslant N_q)$ such that*

$$\left|\omega_{1-\alpha}(t) - \sum_{\ell=1}^{N_q} \varpi^\ell e^{-\theta^\ell t}\right| \leqslant \epsilon \quad \forall\, t \in [\Delta t, T],$$

where the number N_q of quadrature nodes satisfies

$$N_q = O\left(\log\frac{1}{\epsilon}\left(\log\log\frac{1}{\epsilon} + \log\frac{T}{\Delta t}\right) + \log\frac{1}{\Delta t}\left(\log\log\frac{1}{\epsilon} + \log\frac{1}{\Delta t}\right)\right).$$

To be more precise, the Caputo derivative (1.5) is split into the sum of a history part (an integral over $[0, t_{n-1}]$) and a local part (an integral over $[t_{n-1}, t_n]$) at the time t_n. The local part will be approximated by linear interpolation directly; the history part can be evaluated via the SOE technique, that is,

$$\begin{aligned}
(\partial_\tau^\alpha v)(t_{n-\frac{1}{2}}) &\approx \frac{1}{\tau_n}\int_{t_{n-1}}^{t_n}\int_0^{t_{n-1}} v'(s)\sum_{\ell=1}^{N_q}\varpi^\ell e^{-\theta^\ell(t-s)}\,\mathrm{d}s\,\mathrm{d}t \\
&\quad + \frac{1}{\tau_n}\int_{t_{n-1}}^{t_n}\int_{t_{n-1}}^{t} \omega_{1-\alpha}(t-s)(\Pi_1 v)'(s)\,\mathrm{d}s\,\mathrm{d}t \\
&= \bar{a}_0^{(n)}\nabla_\tau v^n + \frac{1}{\tau_n}\sum_{\ell=1}^{N_q}\varpi^\ell\int_{t_{n-1}}^{t_n}\int_0^{t_{n-1}} v'(s)e^{-\theta^\ell(t-t_{n-1})}e^{-\theta^\ell(t_{n-1}-s)}\,\mathrm{d}s\,\mathrm{d}t \\
&= \bar{a}_0^{(n)}\nabla_\tau v^n + \frac{1}{\tau_n}\sum_{\ell=1}^{N_q}\varpi^\ell b^{(n,\ell)}\mathcal{H}^\ell(t_{n-1}), \quad n \geq 1, \qquad (4.1)
\end{aligned}$$

in which

$$\mathcal{H}^\ell(t_k) := \int_0^{t_k} e^{-\theta^\ell(t_k-s)}v'(s)\,\mathrm{d}s \quad \text{with} \quad \mathcal{H}^\ell(t_0) = 0, \quad b^{(k,\ell)} := \int_{t_{k-1}}^{t_k} e^{-\theta^\ell(t-t_{k-1})}\,\mathrm{d}t.$$

By utilizing the linear interpolation and a recursive formula, we can approximate $\mathcal{H}^\ell(t_k)$ by

$$\mathcal{H}^\ell(t_k) \approx \int_0^{t_{k-1}} e^{-\theta^\ell(t_k-s)}v'(s)\,\mathrm{d}s + \int_{t_{k-1}}^{t_k} e^{-\theta^\ell(t_k-s)}\frac{\nabla_\tau v^k}{\tau_k}\,\mathrm{d}s$$

$$= e^{-\theta^\ell \tau_k}\mathcal{H}^\ell(t_{k-1}) + c^{(k,\ell)}\nabla_\tau v^k, \tag{4.2}$$

where the positive coefficients are

$$c^{(k,\ell)} := \frac{1}{\tau_k}\int_{t_{k-1}}^{t_k} e^{-\theta^\ell(t_k-s)}\,\mathrm{d}s, \quad k \geq 1.$$

Having taken this excursion through (4.1)–(4.2), we arrive at the fast L1$^+$ formula

$$(\partial_f^\alpha v)^{n-\frac{1}{2}} := \bar{a}_0^{(n)}\nabla_\tau v^n + \frac{1}{\tau_n}\sum_{\ell=1}^{N_q}\varpi^\ell b^{(n,\ell)}\mathcal{H}^\ell(t_{n-1}), \tag{4.3}$$

where $\mathcal{H}^\ell(t_k)$ is computed by using the recursive relationship

$$\mathcal{H}^\ell(t_k) = e^{-\theta^\ell\tau_k}\mathcal{H}^\ell(t_{k-1}) + c^{(k,\ell)}\nabla_\tau v^k \ \text{ with } \mathcal{H}^\ell(t_0) = 0 \quad \text{for } k \geq 1 \text{ and } 1 \leqslant \ell \leqslant N_q. \tag{4.4}$$

In summary, we use the recurrence relationship (4.4) to update the history part and utilize the fast L1$^+$ formula (4.3) to approximate the L1$^+$ formula $(\partial_\tau^\alpha v)^{n-\frac{1}{2}}$.

4.2. Adaptive time-stepping strategy. In the previous sections, we have proved that the numerical schemes are unconditionally energy stable which implies large time-steps are allowed. Indeed, in simulating the phase field problems such as the coarsening dynamics problems discussed in Example 4.4, an adaptive time-stepping strategy is necessary to efficiently resolve widely varying time scales and to significantly reduce the computational cost. Roughly speaking, the adaptive time-steps can be selected by using an accuracy criterion example as [6] or the time evolution of the total energy such as [24]. We focus on the former and update the time-step size by using the formula [6]

$$\tau_{ada}\,(e, \tau_{cur}) = \tau_{cur}\rho\sqrt{tol/e},$$

where ρ is a default safety coefficient, *tol* is a reference tolerance, and e is the relative error at each time level. The details of the adaptive time-step strategy are recorded in Algorithm 1. Here, the first-order SAV and second-order SAV schemes refer to the L1 formula and Crank–Nicolson method proposed in this article, respectively.

4.3. Numerical examples. The CN-SAV methods (3.9)–(3.10) and (3.11)–(3.12) are examined for the time-fractional MBE model (1.4). Always, we adopt the fast algorithm (4.3) by setting an absolute tolerance error $\epsilon = 10^{-12}$ and cut-off time $\Delta t = \tau_1$ for the SOE approximation. Specifically, the fractional ODE model $\partial_t^\alpha y(t) = f(t)$ is used in Example 4.1 to test the accuracy of L1$^+$ formula (3.6). Let the final time $T \geq 1$; the time interval $[0, T]$ is always divided into two parts, $[0, T_0]$ and $[T_0, T]$, with total N subintervals. We will take $T_0 = \min\{1/\gamma, T\}$, $N_0 = \lceil \frac{N}{T+1-\gamma^{-1}} \rceil$, and apply the graded mesh $t_k = T_0(k/N_0)^\gamma$ in $[0, T_0]$ to resolve the initial singularity. In the remainder interval $[T_0, T]$, we put $N_1 := N - N_0$ cells with random time-steps $\tau_{N_0+k} := (T - T_0)\epsilon_k/S_1$ for $1 \leqslant k \leqslant N_1$, where $\epsilon_k \in (0, 1)$ are the random numbers and $S_1 = \sum_{k=1}^{N_1}\epsilon_k$.

The time accuracy of the proposed methods is mainly focused on for simplicity, and the Fourier pseudo-spectral method is always applied to approximate the space variables having the same spacing in each spatial direction. To examine the CN-SAV

Algorithm 1 Adaptive time-stepping strategy

Require: Set $\tau_1 := \tau_{\min}$. Given ϕ^n and time-step τ_n

Compute ϕ_1^{n+1} by using first-order SAV scheme with time-step τ_n.
Compute ϕ_2^{n+1} by using second-order SAV scheme with time-step τ_n.
Calculate $e_{n+1} = \|\phi_2^{n+1} - \phi_1^{n+1}\|/\|\phi_2^{n+1}\|$.
if $e_{n+1} < tol$ or $\tau_n \leqslant \tau_{\min}$ **then**
    if $e_{n+1} < tol$ **then**
        Update time-step size $\tau_{n+1} \leftarrow \min\{\max\{\tau_{\min}, \tau_{ada}\}, \tau_{\max}\}$.
    else
        Update time-step size $\tau_{n+1} \leftarrow \tau_{\min}$.
    end if
else
    Recalculate with time-step size $\tau_n \leftarrow \max\{\tau_{\min}, \tau_{ada}\}$.
    Goto 1
end if

TABLE 2
Numerical accuracy of $L1^+$ formula (3.6) with $\sigma = 0.8, \gamma = 1$.

N	τ	$\alpha = 0.1$		$\alpha = 0.5$		$\alpha = 0.9$	
		$e(N)$	Order	$e(N)$	Order	$e(N)$	Order
64	2.24e-02	5.90e-03	–	4.65e-03	–	1.10e-03	–
128	1.16e-02	3.39e-03	0.84	2.67e-03	0.84	6.29e-04	0.84
256	5.87e-03	1.95e-03	0.82	1.53e-03	0.82	3.61e-04	0.82
512	2.88e-03	1.12e-03	0.78	8.80e-04	0.78	2.07e-04	0.78

schemes, the maximum norm error $e(N) := \max_{1\leqslant n\leqslant N} \|\phi(t_n) - \phi^n\|_\infty$ is recorded in each run, and the experimental convergence order in time is computed by

$$\text{Order} := \frac{\log\left(e(N)/e(2N)\right)}{\log\left(\tau(N)/\tau(2N)\right)},$$

where $\tau(N)$ denotes the maximum time-step size for total N subintervals.

Example 4.1. Consider the fractional ODE model $\partial_t^\alpha y(t) = f(t)$ with a solution $y = \omega_{1+\sigma}(t)$ and solve the problem until time $T = 1$, where the parameter σ determines the initial regularity of y. The accuracy of $L1^+$ formula (3.6) is examined carefully using the following three scenarios:

(a) $\sigma > 2$ and $\alpha = 0.1$, 0.5, and 0.9 on uniform mesh (see Table 1 in subsection 3.1);
(b) $\sigma < 2$ and $\alpha = 0.1$, 0.5, and 0.9 using the graded parameter $\gamma = 1$ (see Table 2);
(c) $\sigma < 2$ and $\alpha = 0.3$ and 0.7 using different graded parameters $\gamma \geq 1$ (see Tables 3–4).

Table 1 lists the case (a) having smooth solution, while Tables 2–4 record the two cases (b)–(c) having nonsmooth solutions. From these data tabulated in Tables 1–4, one sees that it is accurate of $O(\tau^{\min\{\gamma\sigma,2\}})$ via the following observations: (i) The numerical accuracy is independent of the fractional order $\alpha \in (0, 1)$, and it is second-order accurate for smooth solutions with $\sigma \geq 2$. (ii) On the uniform mesh, the numerical accuracy degenerates to $O(\tau^\sigma)$ when the regularity parameter $\sigma \in (0, 2)$.

TABLE 3
Numerical accuracy of $L1^+$ formula (3.6) with $\alpha = 0.3$, $\sigma = 0.5$.

N	τ	$\gamma = 2$		τ	$\gamma = 4$		τ	$\gamma = 5$	
		$e(N)$	Order		$e(N)$	Order		$e(N)$	Order
64	2.78e-02	6.47e-03	–	2.68e-02	1.21e-03	–	2.62e-02	1.68e-03	–
128	1.53e-02	3.23e-03	1.15	1.38e-02	3.70e-04	1.77	1.30e-02	5.04e-04	1.71
256	7.37e-03	1.63e-03	0.94	6.57e-03	8.15e-05	2.04	6.76e-03	1.55e-04	1.81
512	3.64e-03	8.20e-04	0.97	3.51e-03	2.46e-05	1.91	3.27e-03	3.77e-05	1.95

TABLE 4
Numerical accuracy of $L1^+$ formula (3.6) with $\alpha = 0.7$, $\sigma = 0.5$.

N	τ	$\gamma = 2$		τ	$\gamma = 4$		τ	$\gamma = 5$	
		$e(N)$	Order		$e(N)$	Order		$e(N)$	Order
64	2.76e-02	8.40e-04	–	2.68e-02	3.46e-04	–	2.71e-02	6.66e-04	–
128	1.49e-02	4.20e-04	1.12	1.37e-02	9.47e-05	1.93	1.30e-02	1.80e-04	1.78
256	7.34e-03	2.12e-04	0.97	6.90e-03	2.47e-05	1.95	6.76e-03	4.91e-05	1.98
512	3.65e-03	1.07e-04	0.99	3.47e-03	6.44e-06	1.96	3.26e-03	1.19e-05	1.94

TABLE 5
Numerical accuracy of CN-SAV scheme (3.9)–(3.10) with $\alpha = 0.8$, $\sigma = 0.4$

N	τ	$\gamma = 3$		τ	$\gamma = 5$		τ	$\gamma = 6$	
		$e(N)$	Order		$e(N)$	Order		$e(N)$	Order
64	3.93e-02	4.41e-04	–	4.10e-02	1.21e-04	–	4.40e-02	1.86e-04	–
128	1.94e-02	1.97e-04	1.14	2.17e-02	3.26e-05	2.05	2.08e-02	2.59e-05	2.63
256	9.89e-03	8.57e-05	1.23	1.00e-02	8.57e-06	1.73	1.05e-02	6.43e-06	2.04
512	4.94e-03	3.73e-05	1.20	5.37e-03	2.19e-06	2.19	5.31e-03	1.74e-06	1.92

TABLE 6
Numerical accuracy of CN-SAV scheme (3.11)–(3.12) with $\alpha = 0.8$, $\sigma = 0.4$

N	τ	$\gamma = 3$		τ	$\gamma = 5$		τ	$\gamma = 6$	
		$e(N)$	Order		$e(N)$	Order		$e(N)$	Order
64	3.65e-02	5.15e-04	–	4.54e-02	3.71e-04	–	3.93e-02	4.16e-04	–
128	1.79e-02	1.97e-04	1.36	2.01e-02	8.36e-05	1.83	2.02e-02	9.83e-05	2.17
256	9.77e-03	8.57e-05	1.37	1.07e-02	2.02e-05	2.26	1.07e-02	2.34e-05	2.24
512	4.91e-03	3.73e-05	1.21	5.26e-03	4.85e-06	2.01	5.27e-03	5.61e-06	2.03

(iii) When the solution is nonsmooth, the numerical accuracy reaches $O(\tau^{\gamma\sigma})$ by the graded mesh, and the second-order accuracy would be recovered by choosing $\gamma \geq 2/\sigma$.

Example 4.2. To examine the temporal accuracy of our CN-SAV schemes, consider the time-fractional MBE model $\partial_t^\alpha \phi = -M\left(\varepsilon^2 \Delta^2 \phi - \nabla \cdot f(\nabla \phi)\right) + g(\mathbf{x}, t)$ with $M = 0.1, \varepsilon^2 = 0.5$ for $\mathbf{x} \in (0, 2\pi)^2$ such that it has an exact solution $\phi = \frac{1}{4}\omega_{1+\sigma}(t)\sin(2x)\sin(2y)$. We compare the numerical solution with the exact solution at $T = 1$ below.

In our computation, we take the artificial parameter $\beta = 1$ and the constant $C_0 = 1$, and the space is discretized by using 128×128 meshes. We run the CN-SAV schemes (3.9)–(3.10) and (3.11)–(3.12) by setting a variety of regularity parameters σ. Numerical results are tabulated in Tables 5–6, respectively. Tables 5 and 6 show the numerical results in the worse case of $\sigma < \alpha$. We observe that it is accurate of

TABLE 7
Number of exponentials needed to approximate $w_{1-\alpha}(t)$ in interval $[\Delta t, 10]$.

α	N_q \ Δt / ϵ	10^{-5}	10^{-6}	10^{-7}	10^{-8}
0.1	10^{-12}	89	100	110	121
0.5	10^{-12}	90	100	111	122
0.9	10^{-12}	90	101	112	123

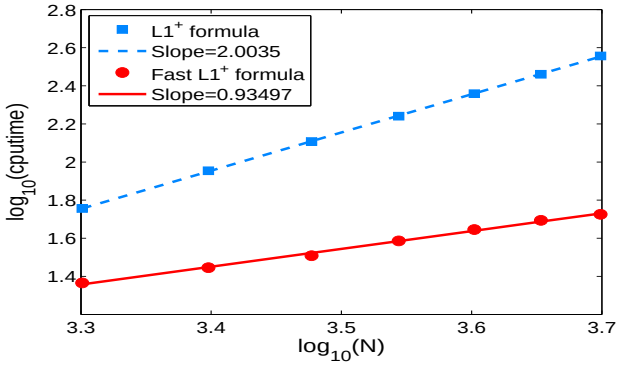

FIG. 2. *The log-log plot of CPU time (in seconds) versus the total number of time-steps N for the CN-SAV scheme* (3.9)–(3.10) *with the L1$^+$ formula* (3.6) *and fast L1$^+$ formula* (4.3). *The slope is obtained by least-square approximation to the CPU time.*

order $O(\tau^{\gamma\sigma})$ on the graded mesh, and the second-order accuracy can be recovered by taking $\gamma \geq \gamma_{\rm opt} = 2/\sigma$. The computational results suggest that it is convergent of $O(\tau^{\min\{\gamma\sigma,2\}})$ in time although no theoretical proof is available up to now.

As stated in Lemma 4.1, for a given absolute tolerance error ϵ, we have the relationship $N_q = O(\log^2(\frac{T}{\Delta t}))$ for $T \approx 1$, and $N_q = O(\log(\frac{T}{\Delta t}))$ for $T \gg 1$ (also see the estimation (1.3) of [10]). To make a conceptional understanding of the actual number N_q needed, Table 7 tabulates the number of exponentials needed to approximate the kernel $w_{1-\alpha}(t)$ in interval $[\Delta t, 10]$. As seen, the number of exponentials needed is moderate even for high accuracy approximation. Meanwhile, in order to demonstrate the efficiency of fast L1$^+$ formula (4.3), we run the CN-SAV scheme (3.9)–(3.10) with the standard L1$^+$ formula (3.6) and fast L1$^+$ formula (4.3) using different time-step numbers N for Example 4.2, respectively. In our computations, we take the spatial grid points 64×64, the SOE parameters $\epsilon = 10^{-12}$ and $\Delta t = 10^{-8}$, and the final time $T = 10$ for the worse case $\alpha = 0.8, \sigma = 0.4$ with the mesh grading $\gamma = 5$. The CPU time (in seconds) plotted in Figure 2 illustrates that the fast L1$^+$ formula (4.3) has the overwhelming performance over the standard L1$^+$ formula (3.6), especially for the large integer N.

Example 4.3. We here examine the performance of the adaptive time-stepping method for the CN-SAV schemes (3.9)–(3.10) and (3.11)–(3.12). To this end, we carry out a standard benchmark problem using initial condition

$$\phi(\mathbf{x}, 0) = 0.1\,(\sin(3x)\sin(2y) + \sin(5x)\sin(5y)) \tag{4.5}$$

with parameter values $M = 1$ and $\varepsilon^2 = 0.1$.

In what follows, we choose the artificial parameter $\beta = 4$, the constant $C_0 = 1$, the safety coefficient $\rho = 0.9$, and the reference tolerance $tol = 10^{-3}$, and the space

$(0, 2\pi)^2$ is discretized by using 128×128 meshes. In addition, let $\tau_{N_0} = \tau_{\min}$ when the graded mesh is applied in initial cell $[0, T_0]$ and adaptive time strategy is employed in the remainder interval $[T_0, T]$, in which the value N_0 is determined by the relationship $\tau_{N_0} = t_{N_0} - t_{N_0-1}$. To quantify the deviation of the height function, define the roughness function $W(t)$:

$$W(t) = \sqrt{\frac{1}{|\Omega|} \int_\Omega \left(\phi\left(\mathbf{x}, t\right) - \bar{\phi}(t)\right)^2 \, \mathrm{d}\mathbf{x}}, \tag{4.6}$$

where $\bar{\phi}(t) = \frac{1}{|\Omega|} \int_\Omega \phi\left(\mathbf{x}, t\right) \, \mathrm{d}\mathbf{x}$ is the average. The function $W(t)$ characterizes the mean size of the network cell.

For a fixed fractional index $\alpha = 0.7$ and final time $T = 30$, we first apply a constant time-step $\tau = 10^{-3}$, i.e., $N = 30000$, to compute the solution. Recall the intrinsically initial singularity of the solution that presented in Figure 1 early; the numerical results suggest the time mesh should be refined near the initial time. As a consequence, we could obtain the reference solution where the parameter values $\gamma = 3, T_0 = 0.01, N_0 = 30$ are applied in the cell $[0, T_0]$ and the uniform mesh is used over the remainder with the total numbers $N = 30000$ as before. For the adaptive time-stepping technique, take the analogous numerical strategy in the initial time and choose parameter $\tau_{\min} = \tau_{N_0} = 10^{-3}$ and $\tau_{\max} = 10^{-1}$ for the remainder.

As a result, time evolutions of the energy and roughness curves for the Slope Model and No-Slope Model are summarized in Figure 3. As can be seen in the figure, the uniform time-step may lead to incorrect steady-state solution while the energies still decay monotonically and the roughness curves show the analogous plots compared with the reference solution. In contrast, we observe that the adaptive energy and roughness curve are practically indistinguishable from the real energy and roughness curves, respectively. Note that the density of circle indicates the size of the adaptive time-step. We then observe that small time-steps are used at the early stage of the computation because of the quick transition of the solution. Subsequently, large time-steps are employed because the solution changes slowly. Again, small time-steps are utilized when capturing the steep structural transition from one stage to the next one. As a consequence, the total numbers of adaptive time-steps are 4443 and 3586 for the Slope Model and No-Slope Model, respectively, while it takes 30000 constant time-steps. The above observations show that the effect of the adaptive time approach on efficiency is significantly dramatic.

Below we make a comparison among different fractional orders α to exploit how the fractional index affects the evolution dynamics. Always, the third time mesh strategy is employed to solve the problem (1.4) with initial condition (4.5) in what follows. Figures 4 and 5 show the plots of the energy and roughness curves of the Slope Model and No-Slope Model for three different values of α. As can be seen from the figures, the initial energy decays rapidly in all cases. Then it will decay slower as the smaller fractional order α. As the time elapses, the evolution dynamics reach the analogous steady state in the end. The above observations may indicate that the time-fractional operator could affect the time scaling of the evolution dynamics, while the steady state may not be affected.

Example 4.4. We investigate the coarsening dynamics using CN-SAV schemes (3.9)–(3.10) and (3.11)–(3.12). The initial condition is a random state by assigning a random number varying from -0.001 to 0.001 to each grid points with parameter value $M = 1, \varepsilon = 0.03$.

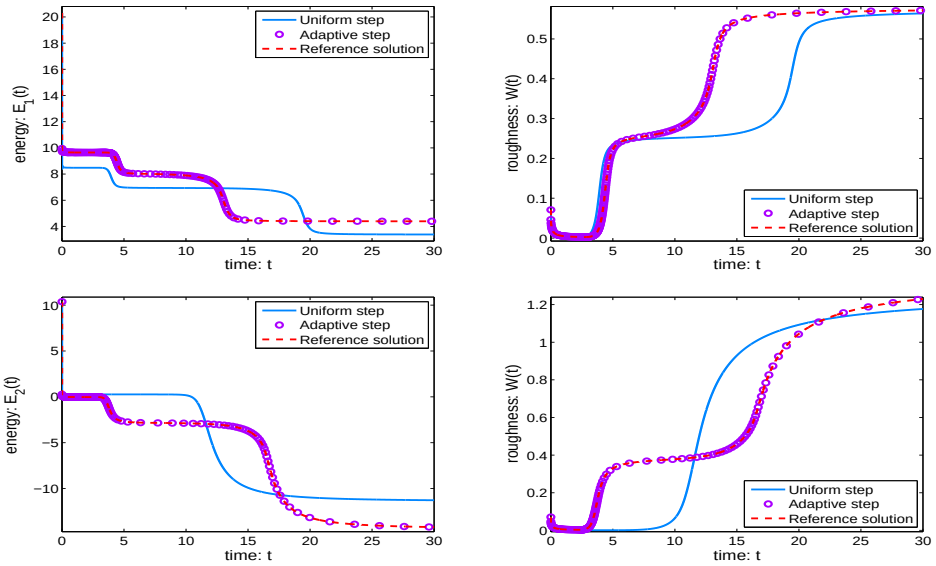

FIG. 3. *Evolutions of modified energy and roughness (from left to right) of the Slope Model and the No-Slope Model (from top to bottom) for* $\alpha = 0.7$ *using different time strategies.*

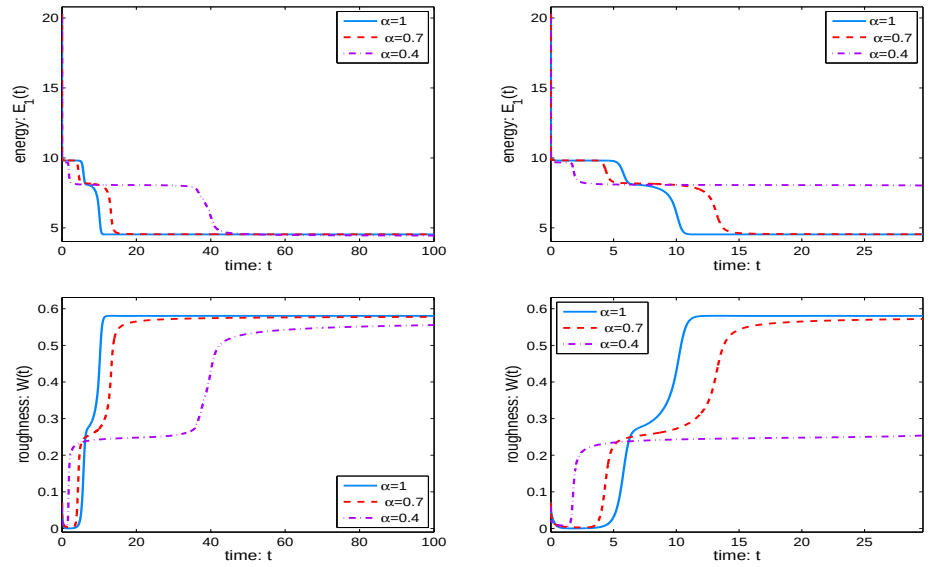

FIG. 4. *Evolutions of modified energy and roughness of the Slope Model (from top to bottom) for* $t \in [0, 100]$ *and* $t \in [0, 20]$ *(from left to right) with* $\alpha = 0.4, 0.7$, *and* 1, *respectively.*

To discover the scaling of effective free energy and roughness in the time-fractional MBE model during coarsening, we use the linear least square fitting to obtain the value of slope for each linear line of roughness, $R(\alpha)$, defined as

$$\log_{10}(W(\alpha,t)) = R^0(\alpha) + R(\alpha)\log_{10}(t),$$

and of energy for the Slope Model, $\beta_1(\alpha)$, and No-Slope Model, $\beta_2(\alpha)$, defined as

$$\log_{10}(E_1(\alpha,t)) = \beta_1^0(\alpha) - \beta_1(\alpha)\log_{10}(t), \quad E_2(\alpha,t) = \beta_2^0(\alpha) - \beta_2(\alpha)\log_{10}(t).$$

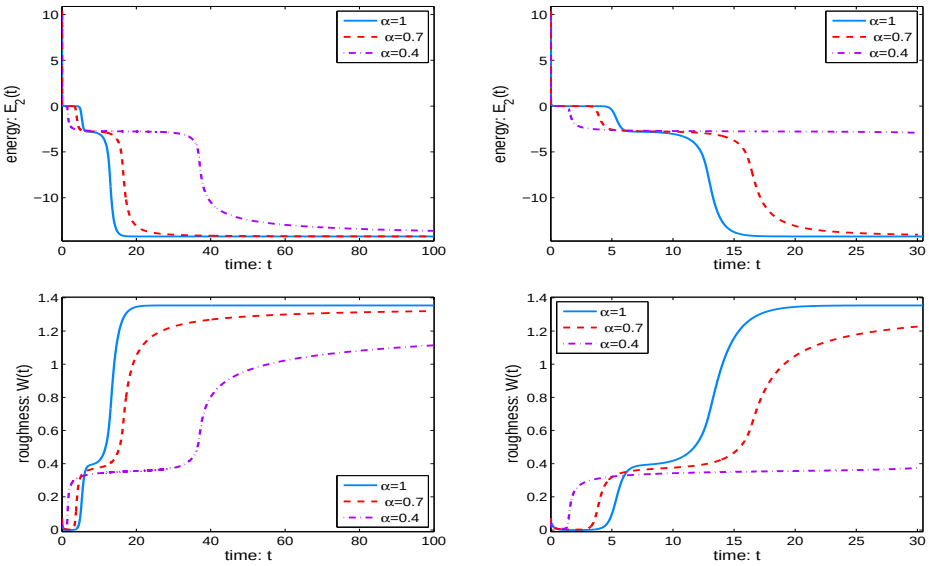

FIG. 5. *Evolutions of modified energy and roughness of the No-Slope Model (from top to bottom) for* $t \in [0, 100]$ *and* $t \in [0, 30]$ *(from left to right) with* $\alpha = 0.4, 0.7,$ *and* 1*, respectively.*

Here $E_1(\alpha, t), E_2(\alpha, t)$, and $W(\alpha, t)$ correspond to the energy $E_1(t), E_2(t)$ and roughness $W(t)$ with the fractional index α, respectively.

In the following computations, we choose the artificial parameter $\beta = 4$, the constant $C_0 = 1$, the initial time $T_0 = 0.01$, the mesh grading $\gamma = 5$, the safety coefficient $\rho = 0.9$, and the reference tolerance $tol = 10^{-3}$. The computational domain $(0, 2\pi)^2$ is discretized by using 128×128 meshes. Figures 6 and 7 show the time evolutions of energy and roughness curves with different fractional orders α for the Slope Model during $t \in [1, 500]$ where the adaptive time-stepping parameters $\tau_{N_0} = \tau_{\min} = 1.25 \times 10^{-4}$ and $\tau_{\max} = 10^{-1}$. We observe that the energy dissipation is approximated as $O(t^{-\frac{\alpha}{3}})$ and the growth rate of the roughness is approximated as $O(t^{\frac{\alpha}{3}})$ which are consistent with consistent with $O(t^{-\frac{1}{3}})$ and $O(t^{\frac{1}{3}})$, respectively, as recorded in [3, 33] for the integer-order Slope Model. The time evolutions of energy and roughness curves for the No-Slope Model using adaptive parameters $\tau_{N_0} = \tau_{\min} = 3.32 \times 10^{-5}$ and $\tau_{\max} = 10^{-1}$ are depicted in Figures 8 and 9, respectively. We observe that the energy dissipation is approximately $O(-\beta_2(\alpha) \log_{10}(t))$ where $\beta_2(\alpha) > 0$ changes linearly with the fractional order α and the growth rate of the roughness is approximately $O(t^{\frac{\alpha}{2}})$ which are consistent with consistent with $O(-\log_{10}(t))$ and $O(t^{\frac{1}{2}})$ as reported in [3, 33] for the integer-order No-Slope Model, respectively.

Furthermore, Figure 10 displays the numerical solutions of the height function ϕ and its Laplacian $\Delta\phi$ for the Slope Model with different fractional orders α. Based on Figure 10 and additional results not shown here for brevity, we observe that the edges of the pyramids generate a random distributed network over the domain and the pyramids become large when the time elapses. Additionally, coarsening dynamics, at the beginning, appear to be faster with smaller α while they would be much slower as the time evolves. Also, the observed phenomena are in good agreement with the published results [34].

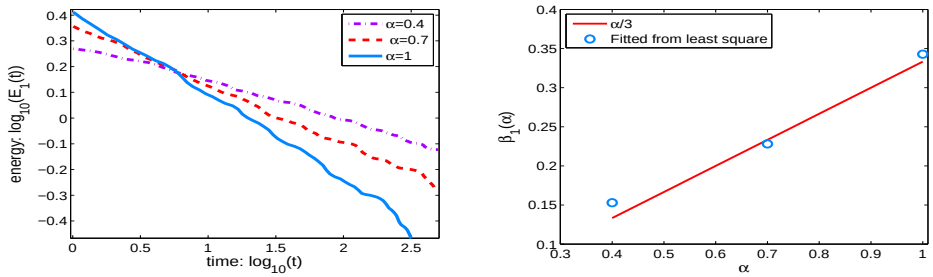

FIG. 6. *The evolution of modified energy (left) and the least square fitted energy dissipation law scaling $\beta(\alpha)$ (right) of the Slope Model for fractional orders $\alpha = 0.4, 0.7$, and 1, respectively.*

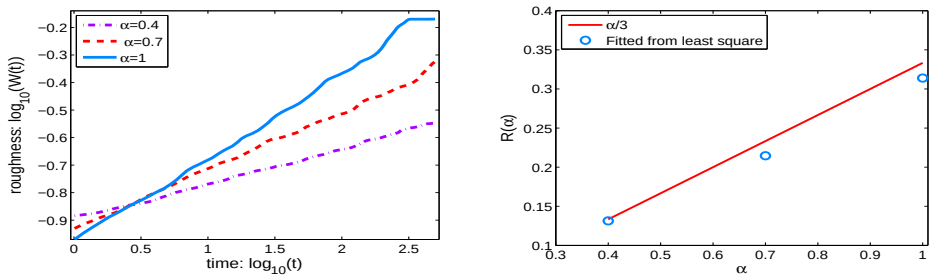

FIG. 7. *The evolution of roughness (left) and the least square fitted roughness growth law scaling $R(\alpha)$ (right) of the Slope Model for fractional orders $\alpha = 0.4, 0.7$, and 1, respectively.*

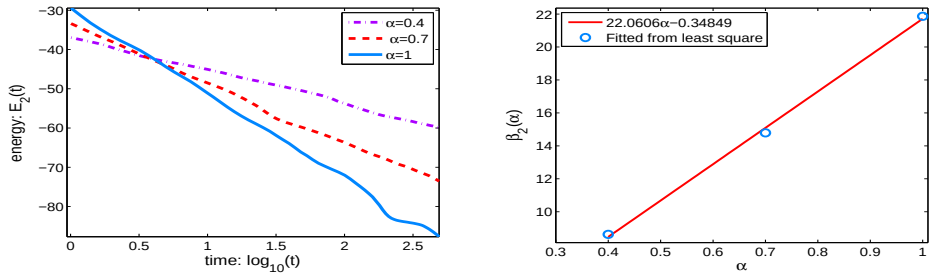

FIG. 8. *The evolution of modified energy (left) and the least square fitted energy decay law scaling $\beta(\alpha)$ (right) of the No-Slope Model for fractional orders $\alpha = 0.4, 0.7$, and 1, respectively.*

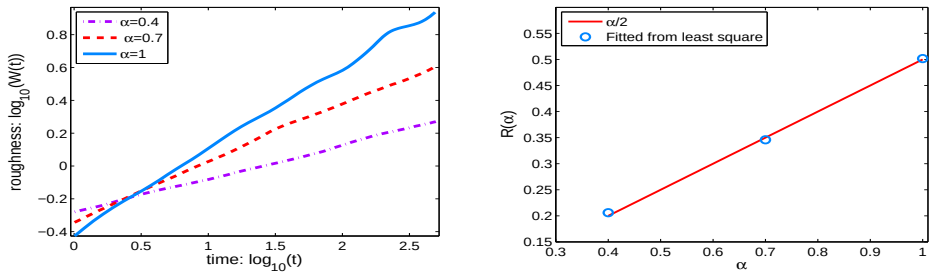

FIG. 9. *The evolution of roughness (left) and the least square fitted roughness growth law scaling $R(\alpha)$ (right) of the No-Slope Model for fractional orders $\alpha = 0.4, 0.7$, and 1, respectively.*

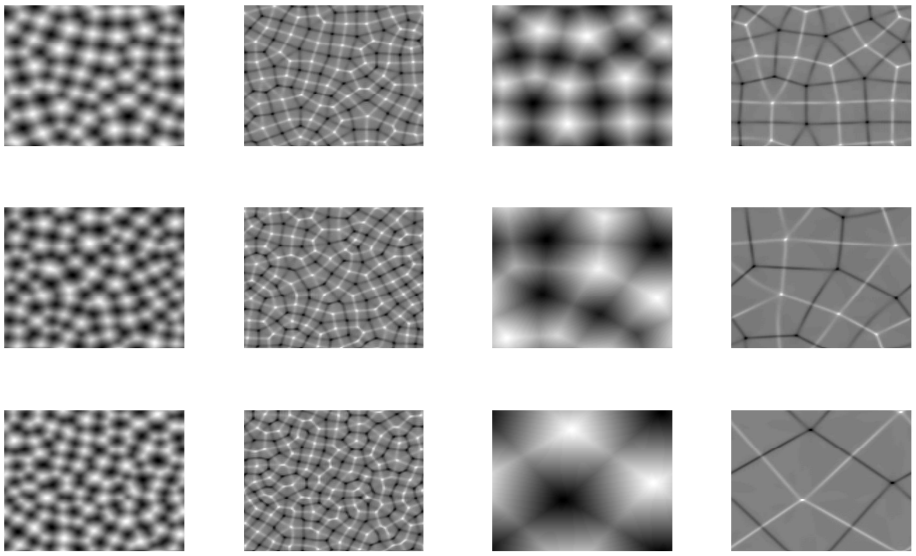

FIG. 10. *The isolines of the height function ϕ and its Laplacian $\Delta\phi$ of the Slope Model with fractional orders $\alpha = 0.4, 0.7$, and 1 (from top to bottom) for $t = 1$ and 500 (from left to right) under random initial condition.*

5. Concluding remarks. In simulating the time-fractional phase field equations including the MBE model considered in this paper, the initial singularity should be treated properly because it always destroys the time accuracy of numerical algorithms especially near the initial time.

It seems challenging to build time-stepping approaches maintaining the discrete energy dissipation law based on the L1 formula, especially on general nonuniform time meshes. Nonetheless, the energy stable schemes permitting adaptive time-stepping strategies are very attractive because they could be applicable for time-fractional phase-field models and for long-time simulations approaching the steady state. As an interesting remedy, the novel L1$^+$ formula is proposed to approximate the fractional Caputo's derivative. As a consequence, we suggest two linearized second-order energy stable CN-SAV schemes for the MBE model with and without slope selection, respectively, by virtue of the SAV approach and the naturally positive semidefinite property of a discrete quadratic form. Furthermore, for the long-time simulations approaching the steady state, the fast L1$^+$ version incorporated with adaptive time-stepping strategy is developed for time-fractional phase field equations. Ample numerical examples are presented to validate the effectiveness of CN-SAV schemes.

The L1$^+$ formula would be superior to some widespread approximations, such as the L1, Alikhanov, and BDF2-like formulas, because it is second-order accurate for both smooth and nonsmooth solutions, and the convergence order is independent of the fractional order $\alpha \in (0, 1)$. Thus it becomes critical to establish the rigorous theory on consistency, stability, and convergence of nonuniform L1$^+$ formula. These issues have been planned for further studies.

Acknowledgments. The authors would like to thank Profs. William McLean, Haijun Yu, and Tao Zhou for their fruitful discussions and suggestions. We also thank the anonymous referees for their valuable comments and suggestions that are very helpful in improving the quality of this article.

REFERENCES

[1] A. Alikhanov, *A new difference scheme for the time fractional diffusion equation*, J. Comput. Phys., 280 (2015), pp. 424–438.

[2] W. Chen, S. Conde, C. Wang, X. Wang, and S. Wise, *A linear energy stable scheme for a thin film model without slope selection*, J. Sci. Comput., 52 (2012), pp. 546–562.

[3] Q. Cheng, J. Shen, and X. Yang, *Highly efficient and accurate numerical schemes for the epitaxial thin film growth models by using the SAV approach*, J. Sci. Comput., 78 (2019), pp. 1467–1487.

[4] S. Clarke and D. Vvedensky, *Origin of reflection high-energy electron-diffraction intensity oscillations during molecular-beam epitaxy: A computational modeling approach.*, Phys. Rev. Lett., 58 (1987), pp. 2235–2238.

[5] G. Gao, Z. Sun, and H. Zhang, *A new fractional numerical differentiation formula to approximate the Caputo fractional derivative and its applications*, J. Comput. Phys., 259 (2014), pp. 33–50.

[6] H. Gomez and T. J. Hughes, *Provably unconditionally stable, second-order time-accurate, mixed variational methods for phase-field models*, J. Comput. Phys., 230 (2011), pp. 5310–5327.

[7] Y. Gong and J. Zhao, *Energy-stable Runge-Kutta schemes for gradient flow models uing the energy quadratization approach*, Appl. Math. Lett., 94 (2019), pp. 224–231.

[8] M. Gyure, C. Ratsch, B. Merriman, R. Caflisch, S. Osher, J. Zinck, and D. Vvedensky, *Level-set methods for the simulation of epitaxial phenomena*, Phys. Rev. E, 58 (1998), pp. 6927–6930.

[9] T. Hou, T. Tang, and J. Yang, *Numerical analysis of fully discretized Crank-Nicolson scheme for fractional-in-space Allen-Cahn equations*, J. Sci. Comput., 72 (2017), pp. 1–18.

[10] S. Jiang, J. Zhang, Z. Qian, and Z. Zhang, *Fast evaluation of the Caputo fractional derivative and its applications to fractional diffusion equations*, Commun. Comput. Phys., 21 (2017), pp. 650–678.

[11] B. Jin, R. Lazarov, and Z. Zhou, *An analysis of the L1 scheme for the subdiffusion equation with nonsmooth data*, IMA J. Numer. Anal., 36 (2016), pp. 197–221.

[12] B. Jin, B. Li, and Z. Zhou, *Numerical analysis of nonlinear subdiffusion equations*, SIAM J. Numer. Anal., 56 (2018), pp. 1–23.

[13] Z. Li, H. Wang, and D. Yang, *A space-time fractional phase-field model with tunable sharpness and decay behavior and its efficient numerical simulation*, J. Comput. Phys., 347 (2017), pp. 20–38.

[14] H.-L. Liao, D. Li, and J. Zhang, *Sharp error estimate of nonuniform L1 formula for time-fractional reaction-subdiffusion equations*, SIAM J. Numer. Anal., 56 (2016), pp. 1112–1133.

[15] H.-L. Liao, P. Lyu, S. Vong, and Y. Zhao, *Stability of fully discrete schemes with interpolation-type fractional formulas for distributed-order subdiffusion equations*, Numer. Algorithms, 75 (2017), pp. 845–878.

[16] H.-L. Liao, W. Mclean, and J.Zhang, *A Second-Order Scheme with Nonuniform Time Steps for a Linear Reaction-Sudiffusion Problem*, e-print, https://arxiv.org/abs/1803.09873v4, 2019.

[17] H.-L. Liao, W. Mclean, and J. Zhang, *A discrete Grönwall inequality with applications to numerical schemes for subdiffusion problems*, SIAM J. Numer. Anal., 57 (2019), pp. 218–237.

[18] H.-L. Liao, Y. Yan, and J. Zhang, *Unconditional convergence of a fast two-level linearized algorithm for semilinear subdiffusion equations*, J. Sci. Comput., 80 (2019), pp. 1–25.

[19] H.-L. Liao, Y. Zhao, and X. Teng, *A weighted ADI scheme for subdiffusion equations*, J. Sci. Comput., 69 (2016), pp. 1144–1164.

[20] H. Liu, A. Cheng, H. Wang, and J. Zhao, *Time-fractional Allen-Cahn and Cahn-Hilliard phase-field models and their numerical investigation*, Comput. Math. Appl., 76 (2018), pp. 1876–1892.

[21] C. Lv and C. Xu, *Error analysis of a high order method for time-fractional diffusion equations*, SIAM J. Sci. Comput., 38 (2016), pp. A2699–A2724.

[22] W. McLean and K. Mustapha, *A second-order accurate numerical method for a fractional wave equation*, Numer. Math., 105 (2007), pp. 481–510.

[23] W. Mclean, V. Thomée, and L. Wahlbin, *Discretization with variable time steps of an evolution equation with a positive-type memory term*, J. Comput. Appl. Math., 69 (1996), pp. 49–69.

[24] Z. Qiao, Z. Zheng, and T. Tang, *An adaptive time-stepping strategy for the molecular beam epitaxy models*, SIAM J. Sci. Comput., 22 (2011), pp. 1395–1414.
[25] J. Shen, T. Tang, and J. Yang, *On the maximum principle preserving schemes for the generalized Allen-Cahn equation*, Commun. Math. Sci., 14 (2016), pp. 1517–1534.
[26] J. Shen, C. Wang, X. Wang, and S. Wise, *Second-order convex splitting schemes for gradient flows with Ehrlich-Schwoebel type energy: Application to thin film epitaxy*, SIAM J. Numer. Anal., 50 (2012), pp. 105–125.
[27] J. Shen and X. Yang, *Numerical approximations of Allen-Cahn and Cahn-Hilliard equations*, Discrete Contin. Dyn. Syst., 28 (2010), pp. 1669–1691.
[28] T. Tang, H. Yu, and T. Zhou, *On energy dissipation theory and numerical stability for time-fractional phase field equations*, SIAM J. Sci. Comput., 41 (2019), pp. A3757–A3778.
[29] J. Villain, *Continuum models of crystal growth from atomic beams with and without desorption*, J. Physique I, 1 (1991), pp. 19–42.
[30] C. Wang, X. Wang, and S. Wise, *Unconditionally stable schemes for equations of thin film epitaxy*, Discrete Contin. Dyn. Syst., 28 (2010), pp. 405–423.
[31] C. Wang and S. Wise, *An energy stable and convergent finite-difference scheme for the modified phase field crystal equation*, SIAM J. Numer. Anal., 49 (2011), pp. 945–969.
[32] C. Xu and T. Tang, *Stability analysis of large time-stepping methods for epitaxial growth models*, SIAM J. Numer. Anal., 44 (2006), pp. 1759–1779.
[33] X. Yang, J. Zhao, and Q. Wang, *Numerical approximations for the molecular beam epitaxial growth model based on the invariant energy quadratization method*, J. Comput. Phys., 333 (2017), pp. 104–127.
[34] J. Zhao, L. Chen, and H. Wang, *On power law scaling dynamics for time-fractional phase field models during coarsening*, Commun. Nonlinear Sci. Numer. Simul., 70 (2019), pp. 257–270.